Polymer 53 (2012) 5404–5412

Contents lists available at SciVerse ScienceDirect

Polymer

journal homepage: www.elsevier.com/locate/polymer

Electrospun isotactic polystyrene nanofibers as a novel β-nucleating agent for isotactic polypropylene

Chi Wang*, You-Ling Chu, Yi-Jiun Wu

Department of Chemical Engineering, National Cheng Kung University, Tainan 701, Taiwan, ROC

ARTICLE INFO

Article history:
Received 5 May 2012
Received in revised form
26 August 2012
Accepted 17 September 2012
Available online 21 September 2012

Keywords:
Electrospinning
Isotactic polystyrene
Transcrystallization

ABSTRACT

Electrospinning of isotactic polystyrene (iPS) solutions at 73 °C or at room temperature was feasibly carried out using *ortho*-dichlorobenzene as the solvent. Depending upon the solution concentration, solution temperature, and collector design, bead-free iPS fibers with diameter of 230–430 nm were successfully obtained. As-spun nanofibers were found to be amorphous and contained oriented iPS chains. The structural evolution of the amorphous iPS nanofibers during stepwise annealing was investigated through two-dimensional small-angle X-ray scattering/wide-angle X-ray diffraction measurements using synchrotron radiation sources. Both the crystal structure (i.e., crystallinity degree and crystal orientation) and lamellar morphology (i.e., lamellar thickness and long period) in the fibers were studied to reveal the possible confinement effect on crystal development. When embedded in the isotactic polypropylene (iPP) matrix, crystalline iPS fibers act as effective nucleating agents that induce iPP transcrystallization on the surface of the fiber. A thin transcrystalline (TCL) layer of α-form iPP crystals is first developed. Subsequent formation of β-form nuclei sporadically takes place at the growing front of α-form TCL, and its growth eventually becomes dominant due to its higher growth rate than the α crystal in the temperature range studied. Having a high surface-to-volume ratio and the ability to induce β-form iPP, electrospun iPS nanofibers act as a promising filler, not only in increasing crystallization kinetics but also in potentially enhancing the toughness of as-prepared nanocomposites.

© 2012 Elsevier Ltd. All rights reserved.

1. Introduction

The development of nucleating agents for isotactic polypropylene (iPP) to yield β-form crystals is important in practical application because the toughness of β-form iPP is higher than that of α form [1]. For decades, several β-nucleating agents have been reported and widely investigated. Some of these agents exclusively produce β-form iPP, whereas some induce α or β-form iPP, depending on the crystallization condition [1,2]. Typical examples for the former are dicyclohexylterephthalamide and γ-quinacridone for the latter to exhibit dual nucleating ability [2]. Epitaxial crystallization of iPP chains on the substrate is proposed and successfully verified for preferential nucleation. Based on the epitaxial consideration [2], dimensional lattice matching between the depositing iPP crystal plane and the substrate with specific periodicity is generally required. A recent study on isotactic polystyrene (iPS) has shown its potential ability to yield β-form iPP when iPS powders with particle size of ~10 μm are added into the iPP matrix [3]. The authors conclude that crystalline iPS powders induce β-form iPP, whereas amorphous iPS powders induce α-form iPP. Moreover, despite its fluidic nature, styrene-related copolymers also exhibit dual nucleating ability toward the iPP matrix in the temperature range of iPP crystallization (110–140 °C) [4]. By contrast, our previous study showed that atactic polystyrene (aPS) fibers are incapable of inducing any iPP crystal, and only α-form iPP is developed at the surface of electrospun syndiotactic polystyrene (sPS) fibers [5]. Several intriguing questions were raised based on these findings. Does the stereo-regularity of PS play a role on fiber nucleating ability toward the crystallization of iPP? Is there any taciticity effect for the PS fibers to yield β-form iPP? What is the mechanism for the formation of β-form iPP on the iPS substrate? To fill this knowledge gap, electrospun iPS fibers were prepared in this study and were used to investigate their nucleating ability toward iPP. Owing to their fine diameter (<1 μm), electrospun fibers provide two advantages compared with conventional fibers with diameter of 10–100 μm. The first advantage is the high surface-area-to-volume ratio, which makes the occurrence of surface-induced crystallization, if any, more efficient. The second advantage is the possession of high fiber modulus and strength due to better chain orientation [6] and less surface defects.

* Corresponding author. Tel.: +886 6 2757575x62645; fax: +886 6 2344496.
E-mail address: chiwang@mail.ncku.edu.tw (C. Wang).

0032-3861/$ – see front matter © 2012 Elsevier Ltd. All rights reserved.
http://dx.doi.org/10.1016/j.polymer.2012.09.036

Electrospinning is a technique used to readily obtain polymer nanofibers by appropriately controlling solution properties (viscosity, conductivity, and surface tension) and processing variables (flow-rate, voltage, and tip-to-collector distance) [7–9]. Most electrospinning processes are carried out at ambient temperatures. However, for some semi-crystalline polymers (i.e., iPS and sPS), which are not easily dissolved in common solvents at room temperature, high-temperature process is required to electrospin the homogeneous solutions. A ribbon-like structure was obtained when dilute iPS solutions (0.5–1.0 wt.%, due to the low solubility at ambient temperature) in choloroform and tetrahydrofuran were used for room-temperature electrospinning [10]. Using electron diffraction, the authors conclude that the skin layer of the ribbons contains some amount of highly-oriented iPS chains, whereas the chains in the interior may be unoriented. To obtain uniform iPS fibers, the network formation by chain entanglements in the electrospinning solution is a general prerequisite. To resolve the solubility issue for electrospinning, a novel facility is recently developed to advance the high-temperature process [11]. This facility includes a heating jacket to maintain the desired temperature of polymer solution, an IR emitter to control environmental temperature, and a laser heating device to locally heat the needle spinneret. Using this set-up, iPS solutions with sufficient concentrations (up to 12 wt%) are feasibly electrospun to form round fibers for further characterization.

In this contribution, the spinnability of iPS solutions with different concentrations and temperatures are studied. Aligned iPS fibers are obtained to investigate the structural variation during stepwise annealing until crystal melting. The possible application of electrospun fibers in the nanocomposite materials is realized by observing the fiber-surface-induced crystallization of the iPP matrix. Despite its fine diameter, electrospun iPS fibers act as effective nucleating agents for the iPP matrix to enhance crystallization rate. More specifically, crystalline iPS fibers exhibit the dual nucleating ability of the α- and β-form iPP, whereas amorphous iPS fibers lose their nucleating ability toward iPP. The mechanism for the formation of β-form iPP is revealed.

2. Experimental

2.1. Electrospinning process

Pellets of iPS with a molecular weight (M_w) of 400,000 g/mol were purchased from Scientific Polymer Products, Inc. *Ortho*-dichlorobenzene (*o*-DCB) purchased from TEDIA Co. was used as solvent in preparing electrospinning solutions. A soluble salt of tetra-n-butylammonium perchlorate (Bu_4NClO_4) obtained from TCI Co. was added into the iPS/o-DCB solution to enhance solution conductivity. Homogeneous iPS solutions with concentration of up to 12 wt% were readily obtained at 160 °C for 2.5 h. The added slat was about 0.5 wt% relative to the amount of solvent used.

A needle with an inner and outer diameter of 0.33 and 0.64 mm, respectively, was used as the spinneret during the electrospinning. A homemade jacket-type heat exchanger was used to maintain the polymer solution at 130 °C through the circulation of heated silicone oil by a pumping system connected to an oil bath [11]. A significant temperature difference was detected between the solutions within the jacket tube and at the needle end because of the thin needle used. By measuring the temperature of the pendent drop at the needle end using a thermocouple, the working temperature of the solution for electrospinning was determined to be 73 °C. When the system reached thermal equilibrium, the homogeneous polymer solution was electrospun into fiber forms. The prepared solution was delivered by a syringe pump (Cole–Parmer) into the needle at a controlled flow-rate of 1.0 mL/h. A positive voltage of 18 kV was applied from a high-voltage source (Bertan, 205 B) to provide sufficient electric field for electrospinning. A stationary steel net (30 × 30 cm^2) was used as a collector for the electrospun fibers at a fixed tip-to-collector distance of 21 cm. The collected iPS fibers showed non-woven fabric character based on the stationary plate. Aligned fibers were collected using a rotating disc (diameter of 10 cm, width of 5 mm) with a linear velocity of 18.8 m/s. Detailed processing conditions were provided in our previous paper [11]. For the present iPS/*o*-DCB solutions, a stable cone-jet electrospinning mode was maintained for hours without interruption. The morphology of the as-spun fibers was observed using a scanning electron microscope (SEM, Hitachi S4100). Fiber diameters were measured within electron micrographs from a population of ~500 fibers, from which the average fiber diameter and the corresponding standard error were determined. Differential scanning calorimetry (DSC) thermogram was obtained using a DSC (Perkin Elmer, DSC7) under nitrogen atmosphere at a scanning rate of 10 °C/min.

2.2. Structural development of iPS fibers during annealing

Aligned fibers electrospun from the 12 wt% iPS solution were used to characterize structural evolution during stepwise heating. A Mettler stage (FP900) was used for temperature control. The heating process was realized by a stepwise increase of temperature from 35, 85, 95, 100, 110, 120, 140, 180, 200–225 °C per step and a holding time of 6 min each for data acquisition. During heating, two-dimensional (2-D) small-angle X-ray scattering (SAXS) and wide-angle X-ray diffraction (WAXD) measurements were conducted at the wiggler beamline BL23A and BL17A, respectively, from the National Synchrotron Radiation Research Center (NSRRC) in Taiwan, with an 8 keV (wavelength $\lambda = 0.155$ nm) beam. Specimens were sealed in Al pans with Kapton windows ca. 2 mm in diameter for the X-ray beam. All X-ray data were corrected for beam fluctuations, sample absorption, and background scattering. Details of the experimental setup and data analysis can be found elsewhere [12]. Gaussian functions were used to describe the crystal reflections and the amorphous phase during the deconvolution of the WAXD curves to determine fiber crystallinity. Based on the distribution plot of WAXD intensity along the azimuthal direction, the orientation factor of the induced crystals was determined using the Herman orientation function [13]:

$$f = \left(3 < \cos^2\phi_{hkl,Z} > - 1\right)/2 \tag{1}$$

where $< \cos^2\phi_{hkl,z} >$ is the squared average of the cosine value of the angle, $\phi_{hkl,z}$, between the normal of the (*hkl*) plane with the fiber axis (*Z* axis). The quantity can be experimentally derived using the following equation:

$$< \cos^2\phi_{hkl,Z} > = \int_0^{\pi/2} I_{hkl}\left(\phi\right)\cos^2\phi \sin\phi \mathrm{d}\phi \Big/ \int_0^{\pi/2} I_{hkl}(\phi)\sin\phi \mathrm{d}\phi \tag{2}$$

where $I_{hkl}(\phi)$ is the intensity distribution of the (*hkl*) plane on the Debye ring and ϕ is the azimuthal angle measured from the meridian (fiber axis direction). Since the iPS crystals possess hexagonal symmetry, the crystal *c*-axis orientation, $f_{c,Z}$, could be determined from the following (*hk0*) intensity profile [13]:

$$< \cos^2\phi_{c,Z} > \; = \; 1 - 2 < \cos^2\phi_{hk0,Z} > \tag{3}$$

Perfect crystal orientation leads to $f_{c,Z}$ value of 1.0, whereas perpendicular crystal orientation gives rise to a value of −0.5. The value of $f_{c,Z}$ is 0 in random crystal orientation. In this study, the strong reflection of (220) plane was selected to deduce the $f_{c,Z}$ value. The intensity profiles along the azimuthal direction at different T_a

are shown in Figure S1 (supplementary materials), from which the $f_{c,Z}$ values were derived by Eqs. (1)–(3).

To analyze SAXS data, the intensity profile along the meridian was extracted. The scattering intensity at high scattering vector q ($= 4\pi\sin\theta/\lambda$, where 2θ is the scattering angle) was corrected according to Porod's law [14]. Lorentz-corrected curve was constructed by plotting $q^2I(q)$ versus q. SAXS scattering peak indicated the presence of a regular long period of iPS lamellar stacks. From the peak position of q_m, the long period (L_B) was estimated by $2\pi/q_m$ based on Bragg's law. Linear correlation functions $\gamma_1(r)$ were also calculated to examine the detailed lamellar structures [14]:

$$\gamma_1(z) = \int_0^\infty q^2 I(q)\cos(qz)\mathrm{d}q \Big/ \int_0^\infty q^2 I(q)\mathrm{d}q \tag{4}$$

The correlation functions contain the basic morphological information of a lamellar stack model, from which three characteristic lengths (L_c, z_1, and z_2) are derived. The long period L_c is directly obtained from the position of the first maximum. Further analysis of $\gamma_1(r)$ gives rise to two lengths (z_1 and z_2) [14–16], namely, average crystalline lamellar thickness l_c and amorphous layer thickness l_a, with $L_c = l_c + l_a$. According to Babinet's principle of reciprocity, correlation analysis alone is not feasible to determine which length corresponds to l_c and l_a. Considering that the linear crystallinity ϕ_{cl} ($=l_c/L_c$) within the lamellar stacks should not be smaller than the apparent crystallinity determined by DSC (or WAXD), smaller length (z_1) was assigned to l_c in agreement with previous findings by Strobl et al. [15] and Cebe et al. [16].

The Fourier-Transform Infrared (FTIR) spectra of the aligned fibers during stepwise annealing were obtained at different temperatures using a Perkin Elmer Spectrum 100 spectrometer with a resolution of 2 cm^{-1} and 64 scans. The fibers were shed by the polarized IR light with the electric vector parallel and perpendicular to the fiber axis to obtain the respective absorbances, i.e. $A_{//}$ and $A_{\perp}$. Then, the dichroic ratio ($A_{//}/A_{\perp}$) was derived to estimate the orientation of iPS chains.

2.3. Electrospun-fiber-induced transcrystallization of iPP

The same batch of iPP powder used for our previous transcrystallization studies [5] was applied in this work, which had a viscosity average molecular weight of 2.8×10^5 g/mol. The testing fibers were covered with iPP powders and placed in a well-controlled hot stage (Linkam, THMS600) at a temperature of 200 °C for 10 min to homogenize the iPP melts. The samples were then cooled at different rates (4–60 °C/min) to room temperature. Dry nitrogen was introduced to eliminate plausible thermal degradation. Crystallization of iPP on the iPS fibers was monitored with a polarized optical microscope (POM, Leica DMLP) equipped with phase contrast lens. WAXD intensity profile of the crystallized samples was obtained and the following equation, proposed by Turner-Jones et al. [17], was applied to estimate the content of β-form iPP (K_β) induced by the iPS fibers:

$$K_\beta = I_{\beta(300)} \Big/ \left[I_{\beta(300)} + I_{\alpha(110)} + I_{\alpha(040)} + I_{\alpha(130)}\right] \tag{5}$$

where $I_{\beta(300)}$ is the intensity of the (300) reflection peak of the β-form, and $I_{\alpha(110)}$, $I_{\alpha(040)}$, and $I_{\alpha(130)}$ are the intensities of the (110), (040), and (130) reflection peaks of the α-form, respectively.

3. Results and discussions

3.1. Morphology of electrospun iPS fibers

The iPS solutions in the entangled regime are generally required to obtain bead-free fibers by electrospinning [18]. A simple formula, namely, $\phi_e \sim 2M_e/M_w$, is available to estimate the entanglement concentration (ϕ_e), where M_e is the entanglement molecular weight for undiluted iPS melt (27,200 g/mol) [19]. For the present iPS, the ϕ_e was calculated to be 13.6 vol.% (or 11.4 wt%). Fig. 1 shows the products obtained from the electrospinning of solutions with different iPS concentrations and collecting methods. Evidently, beaded fibers were obtained from the 8 wt% iPS solution, whereas uniform iPS fibers were electrospun from the solutions with a concentration of 10 wt% or higher, which is in fair agreement with the theoretical prediction. At a given electrospinning temperature of 73 °C, the diameter of as-spun iPS fibers increased with increasing solution concentration, mainly due to the solution viscosity effect. The cooled iPS solutions were found to remain homogeneous even at room temperature for hours due to the slow process of gel formation and/or crystallization, which led to the feasibility of ambient electrospinning. However, thick fibers were obtained by electrospinning at a lower temperature. For example, electrospinning of the 12 wt% solution at 73 °C produced fibers with diameter of 379 ± 58 nm, but room temperature process gave rise to iPS fibers with diameter of 433 ± 72 nm. Thus, fibers electrospun from the elevated temperature had lower diameter than those obtained from room temperature because of reduced viscosity. We conclude that solution concentration and temperature are two controlling parameters associated with solution viscosity, which could be used to manipulate fiber diameter. Using a rotating disc as a collector enabled iPS fibers aligned with a reduced diameter of 325 ± 74 nm to be obtained from the room temperature electrospinning of the 12 wt% solution. The additional fiber reduction is attributed to the extra stretching of the depositing fibers, provided that the linear velocity of the rotating disc is higher than the jet whipping velocity. Notably, the feasibility of room temperature electrospinning for the present iPS/*o*-DCB solution is attributed to the slow crystallization (or gelation) process at ambient temperature. This phenomenon is in great contrast with the sPS/*o*-DCB solution, where electrospinning is performed at temperatures higher than 90 °C to keep the solution in homogeneous state [20].

3.2. Structural evolution of electrospun iPS fibers during heating

Fig. 2 shows the 2-D WAXD/SAXS patterns of iPS fibers annealed at three selected T_a of 35, 120, and 200 °C (the rest are provided in Figures S1 and S2). The corresponding intensity profiles are shown in Fig. 3, in which the WAXD profiles are obtained from the radial average, whereas the SAXS profiles are deduced from the slice along the meridional direction. The as-spun fibers exhibited two broad amorphous halo centered at $2\theta = 9.0°$ and 18.8°, yielding Bragg spacing of 0.981 and 0.471 nm, respectively. The former was associated to the inter-chain distance and the latter to the inter-benzene distance. The small reflection peak at $2\theta = 8.4°$ was associated to the added salt [11]. Upon heating, no detectable crystalline peak was observed until $T_a = 110$ °C, where the typical reflection peaks associated with the iPS crystals were first seen. The intensity of reflection peaks became stronger at higher T_a, suggesting the occurrence of cold crystallization. Based on the hexagonal modification, the WAXD peaks located at $2\theta = 7.9$, 13.7, 15.8, 18.0, 21.2, 23.8, and 27.4° were indexed to the planes of (110), (300), (220), (211), (410), (330), and (012), respectively [21]. After the de-convolution of the intensity profile, the fiber crystallinity (ϕ^{WAXD}) was determined from the integrated area of crystalline peaks to the total area. The WAXD results indicate that ϕ^{WAXD} increased in T_a of 100–140 °C, followed by a mild increment until 200 °C. Rapid crystal melting took place afterward. As regards the SAXS profiles, a scattering peak was first seen at 140 °C, a temperature higher than that to detect the initial iPS crystals by WAXD. This mechanism demonstrated that iPS hexagonal crystals develop prior to the formation of iPS lamellar stacks, following the classical

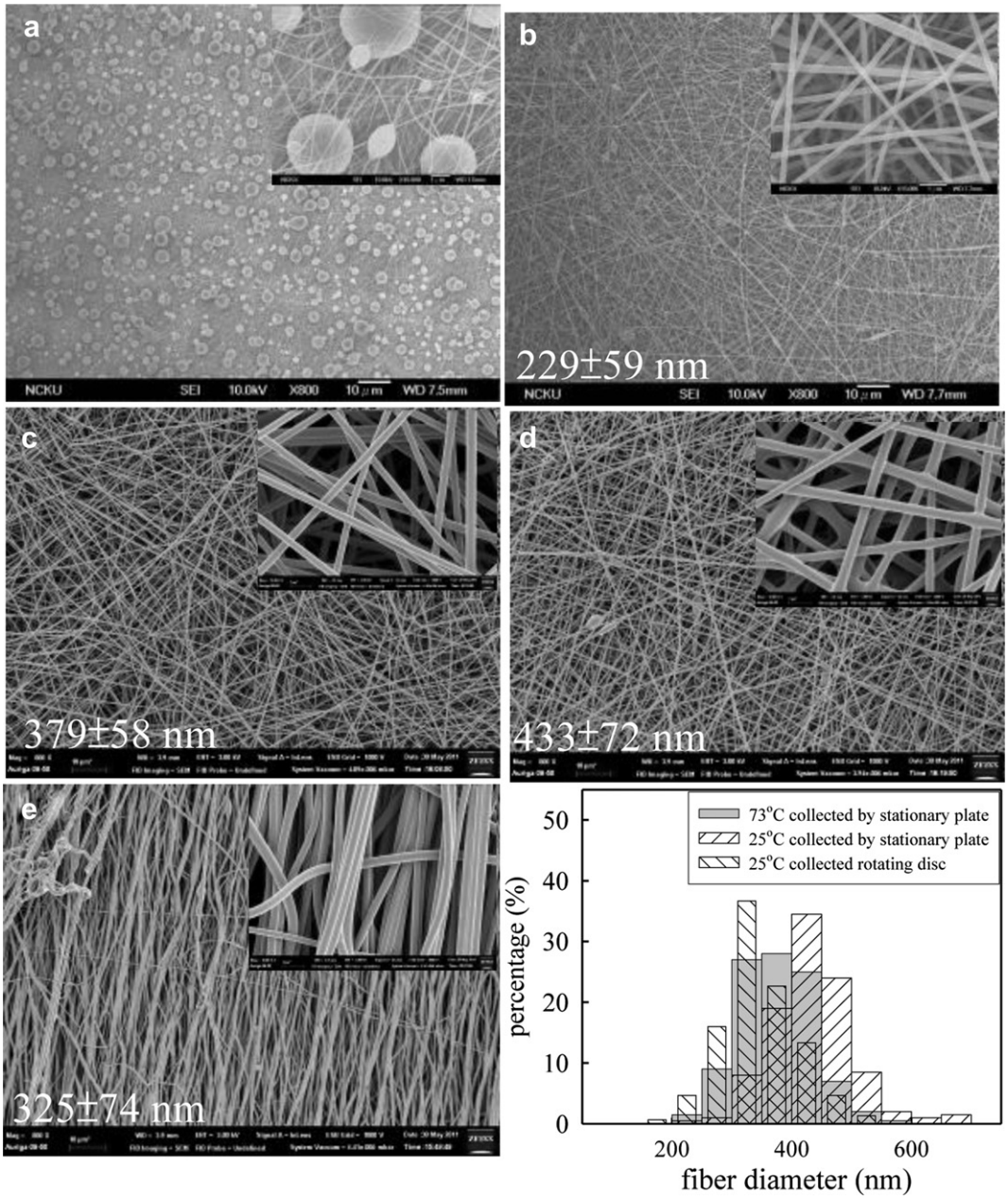

Fig. 1. SEM images of as-spun iPS fiber morphology; (a), (b) (c) are products electrospun at 73 °C and collected by a stationary plate from solutions of 8, 10 and 12 wt% iPS, respectively. (d) And (e) are fibers electrospun from the 12 wt% solution at 25 °C, collected by a stationary plate and by a rotating disk, respectively. For the 12 wt% solution-spun fibers, the fiber diameter histograms are displayed for comparison.

crystallization kinetics of "nucleation and growth kinetics". It contrasts with the crystallization of iPP chains in the electrospun fibers through the intermediate mesomorphic phase [11]. As T_a is elevated, a marked increase in the SAXS intensity and a shift of the SAXS maximum to smaller q are observed. The shift corresponds to an increase of the long period with increasing annealing temperature. The position of the scattering peak was used to determine the L_B based on Bragg's law. Fig. 4 shows the T_a-dependence of ϕ^{WAXD} and L_B, together with the morphological parameters (L_c, l_c, and l_a) determined from the correlation function analysis. The L_B was derived for the sample at 140 °C, but analysis of the correlation function was too difficult to perform due to its weak SAXS intensity. Consistent with the previous reports [14], L_B is larger than L_c obtained by the correlation function. Also included in Fig. 4 is the DSC heating scan of the aligned iPS fibers at a rate of 10 °C/min, which shows a glass transition temperature (T_g) of 94.2 °C, a cold crystallization temperature of 149.3 °C, and a melting temperature of 224.5 °C. The enthalpy change associated with the crystallization exotherm was 15.6 J/g, which was lower than that of the melting endotherm at 21.4 J/g. Using the reported value of 86.6 J/g for the 100% crystalline iPS [21], the fiber crystallinity induced by 10 °C/min heating was estimated to be 0.247. Careful examination of the curve revealed the initial temperatures for cold crystallization and crystal melting to be 117.1 and 206.3 °C, respectively. No melt-crystallization event was seen on cooling from 260 °C due to the slow crystallization process of iPS (Figure S3). The second heating curve did not exhibit cold crystallization but demonstrated a melting peak at 222.0 °C instead. However, the melting enthalpy was only 4.14 J/g, which was much lower than that of the 1st heating run. Based on the melting line concept [15], Al-Hussein and

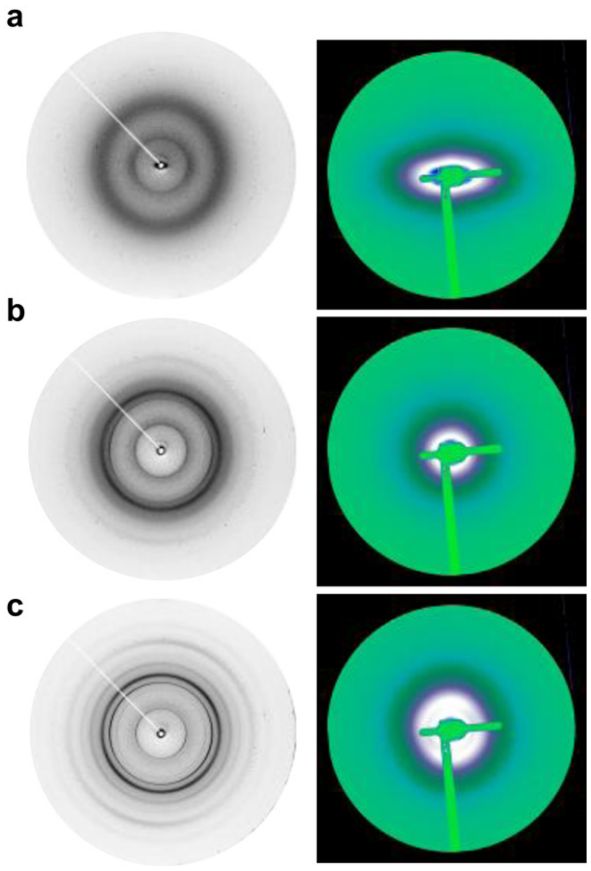

Fig. 2. Selected 2-D WAXD (left column) and 2-D SAXS (right column) of aligned iPS fibers at different temperatures (a) 35, (b) 120, and (c) 200 °C during stepwise annealing. The fibers are obtained from room-temperature electrospinning of 12 wt% solution, and are collected by a rotating disk. The fiber direction is vertical.

Strobl determined the equilibrium melting temperature of iPS crystals to be 289 ± 5 °C. We speculate that traced amount of residual nuclei survive at a melt temperature of 260 °C and they become activated during cooling and subsequent heating traces. However, the exothermic event for the crystallization is too subtle to be detected by the present DSC used. These findings indicate the slow crystallization kinetics of non-oriented iPS chains under common thermal treatment (i.e., melt, cooling and heating at 10 °C/min). By contrast, the as-spun amorphous iPS fibers readily crystallized because of the oriented chain conformation induced by the electrospinning process.

Two major processes take place during the heating of amorphous iPS fibers with oriented chains: chain relaxation and cold crystallization processes. Crystals with high orientation emerge provided that the crystallization kinetics is faster than the relaxation process. In the case where crystallization kinetics is slower than the relaxation process, the oriented chains dramatically relax first, and subsequent crystallization gives rise to crystals with less orientation. To quantitatively characterize the orientation of amorphous chains prior to crystallization, polarized IR spectroscopy was applied. Fig. 5 shows selected IR spectra of the aligned fibers obtained during stepwise annealing from 35 to 140 °C. The derived dichroic ratio of the 909 cm^{-1} band was used to estimate the orientation of the amorphous chains, whereas those of 899, 920, 981 and 1051 cm^{-1} bands represented the orientation of iPS crystallites [22]. At 35 °C, the crystal-related bands were absent and the determined dichroic ratio of 909 cm^{-1} band was 2.08, indicating a preferential orientation of amorphous chains developed in the as-spun fibers. Increasing T_a leads to the reduction of the dichroic ratio of 909 cm^{-1} band; being 1.72, 1.44, 1.35 and 1.21 at T_a = 85, 95, 100, and 110 °C, respectively. At T_a = 120 °C, the formation of iPS crystals was validated by the appearance of crystalline-sensitive band at 908 cm^{-1}. This evidence concludes that the relaxation of oriented amorphous iPS chains occurs prior to cold crystallization. At a higher T_a of 140 °C, fibers crystallinity was increased and the developed iPS crystals exhibited a preferential orientation since both the crystal-related bands of 920 and 1051 cm^{-1} are more intense in the perpendicular spectrum.

Based on the data shown in Figs. 4 and 5, the structural evolution in the as-spun fibers is concluded as follows. The as-spun iPS fibers are amorphous. A small fraction of iPS hexagonal crystals (~0.049) is initially seen by WAXD during heating at 110 °C.

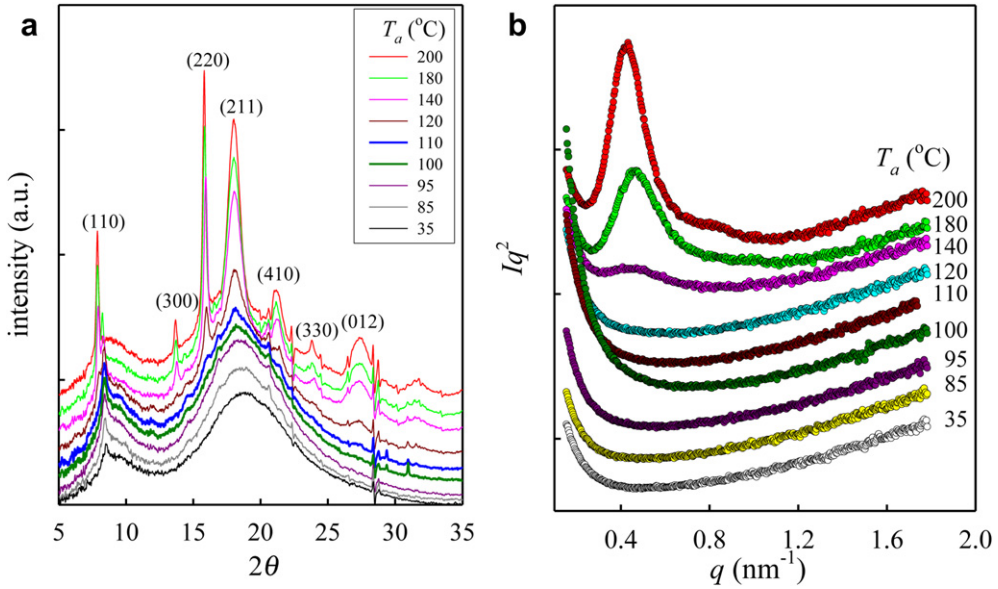

Fig. 3. (a) WAXD, (b) SAXS intensity profiles of iPS fibers during stepwise annealing. WAXD profiles are obtained from the radial average intensities of the 2-D patterns, and SAXS curves are obtained from the slice along the meridian. The temperatures from bottom to top are: 35, 85, 95, 100, 110, 120, 140, 180, and 200 °C. In (a), the small reflection peak at $2\theta = 8.4°$ is associated to the added salt of Bu_4NClO_4. Each curve is vertically shifted for a better comparison.

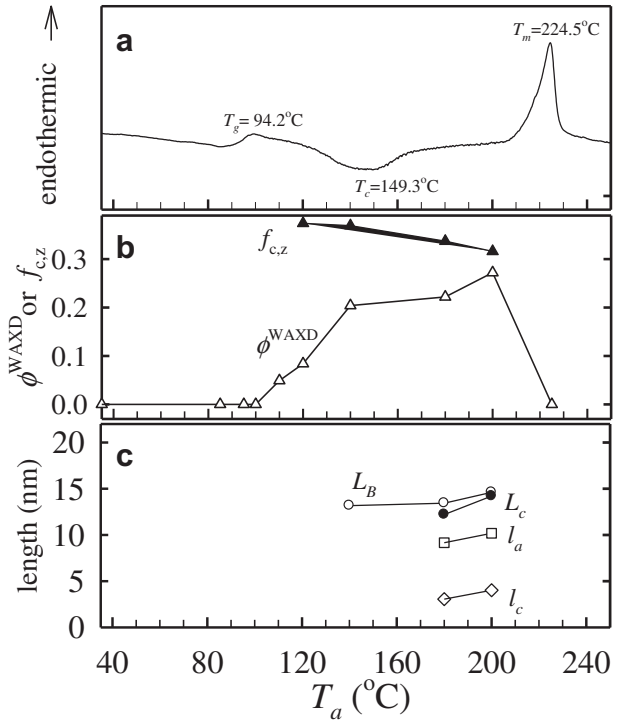

Fig. 4. (a) DSC heating trace on the as-spun iPS fibers at a rate of 10 °C/min. During stepwise annealing at various temperatures of T_a, the variation of (b) Fiber crystallinity ϕ^{WAXD} and c-axis orientation factor of iPS crystal $f_{c,z}$, and (c) Long periods L_B, L_c determined from the Bragg's law and the correlation function, respectively, together with the lamellar thickness l_c and amorphous layer thickness l_a derived from the correlation function.

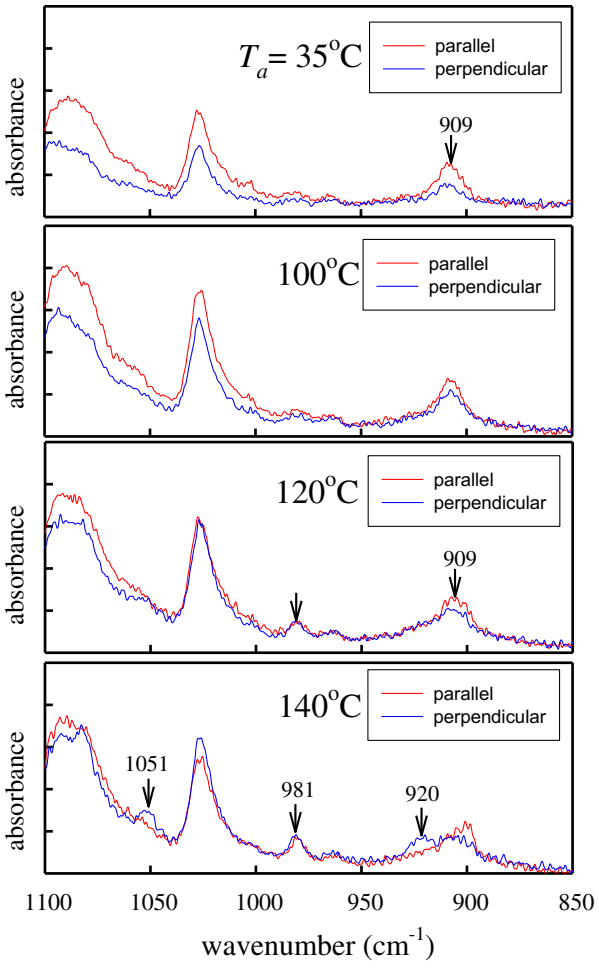

Fig. 5. Polarized IR spectra of the aligned iPS fibers during stepwise annealing at 35, 100, 120, and 140 °C, respectively. Parallel and perpendicular polarizations are indicated by the red and blue lines, respectively. The 909 cm^{-1} band is associated with amorphous chains, whereas bands 899, 920, 981 and 1051 cm^{-1} are relevant with the crystallites (For interpretation of the references to colour in this figure legend, the reader is referred to the web version of this article.)

Continuous heating up to 140 °C leads to the rapid ϕ^{WAXD} increase to reach a value of 0.204, and lamellar structure is first detected with L_B of 13.17 nm. In this T_a range, the crystal orientation of $f_{c,Z}$ remains constant at 0.37. Further annealing to 200 °C brings up a mild ϕ^{WAXD} increase to reach the maximum value of 0.272, whereas $f_{c,Z}$ is gradually reduced to 0.32, suggesting that the newly developed iPS crystals are less oriented. In this T_a range, the lamellar thickness is slightly increased from 3.05 nm at 180 °C to 4.02 nm at 200 °C. The obtained l_c is slightly lower than that crystallized from the amorphous iPS chains in a randomly oriented state, yielding an l_c of 3.6 nm at 180 °C, and 4.5 nm at 200 °C [15]. The corresponding ϕ_{cl} value is 0.250 at 180 °C and becomes 0.273 at 200 °C, which are similar to those obtained from WAXD and DSC. Thus, a consistent agreement is reached to validate the lamellar stack model for the internal structure of iPS fibers upon annealing. Notably, less crystal orientation takes place in the annealed iPS fibers compared with the annealed sPS fibers possessing a high value of $f_{c,Z}$ (ca. 0.97) [20] determined by electron diffraction. The formation of highly oriented crystals in the sPS fibers is attributed to the fast crystallization of sPS chains so that chain relaxation is depressed upon heating. By contrast, the iPS chains in the as-spun fibers undergo dominant relaxation, followed by slow crystallization kinetics, thereby giving rise to the formation of less-oriented iPS crystals. In other words, the chain relaxation process outperforms the cold crystallization process on heating the as-spun iPS fibers. Alternative evidence is evidently obtained in Fig. 4a and b, in which the main crystallization evolution shifts to a higher temperature range using a heating rate of 10 °C/min, compared with that by stepwise heating.

The presence of microvoids developed in the as-spun iPS fibers is the final topic for 2-D SAXS patterns (Fig. 2 and S2), as evidenced by the strong zero-angle scattering along the equator. The oval-shaped SAXS pattern suggests that the elongated microvoids orient along the fiber axis. This unique scattering feature could be also observed from the 2-D WAXD pattern near the beam stopper (Figure S1). Microvoids have often been reported in the conventional dry or wet spinning process, in which solvents are involved [23]. Upon annealing the as-spun iPS fibers, no change of the zero-angle scattering pattern is observed until T_a of 100 °C, which is higher than the T_g of iPS, at which oriented amorphous iPS chains start to relax. Chain relaxation in the vicinity of the microvoids leads to the shape change of microvoids, which become more spherical, revealing the symmetric pattern of the zero-angle scattering. At T_a = 110 °C and higher, iPS crystallization takes place and the size and shape of microvoids are locked until major crystal melting at 225 °C, where chain mobility is significantly enhanced and zero-angle scattering is diminished due to the disappearance of microvoids.

3.3. Electrospun-fiber-induced crystallization of iPP

The addition of fibers in the semicrystalline matrix not only improves the mechanical properties but may also alter the crystalline structure of the matrix. The formation of TCL layer on the fiber surface is essentially desirable in tailoring interfacial strength.

Despite the submicron diameter, the electrospun iPS fiber preferentially induces the nucleation of iPP at its surface, as shown in Fig. 6a, through a cooling process at a rate of 4 °C/min from 200 °C. Crystalline iPS fibers are developed after this thermal treatment, and the fiber crystallinity is observed at ca. 0.28 (Fig. 4b). Under POM observation, highly birefringent β-form crystals are easily identified, in contrast to the weakly birefringent α-form iPP having lamellar branching structure. Both the α/β-iPP crystals are observed around the iPS fiber. The existence of β-form crystal was also verified by WAXD, as shown in Fig. 7, where a strong reflection of the (300) plane of β-form is clearly observed. The calculated K_β value is 0.54, indicating moderate activity of electrospun iPS fibers to induce β-form iPP [1]. Selective melting of β-form crystal at 153 °C (Fig. 6b and c) reveals that a thin TCL of α-form iPP remains at the fiber section, where the β-form crystals disappear. This finding indicates the presence of overgrown β-form on the growing front of α-form TCL, which nucleates at the fiber surface. Furthermore, this result indicates the occurrence of "α/β bifurcation growth of iPP crystals" [1,24] at the iPS fiber surface. A similar phenomenon has been reported for the iPP chain crystallization on the surface of β-nucleating agent of *N,N'*-dicyclohexyl-2,6-naphthalenedicarboxamide [24]. Thus, the formation of β-form crystal is not heterogeneous, but kinetically favored by the higher growth rate of β-form than that of α-form crystal. The α-form iPP is thermodynamically more stable than the β-form, but its crystal growth rate is lower than that of the β-form in the major temperature range between $T_{\alpha\beta}$ (~105 °C) and $T_{\beta\alpha}$ (~141 °C) [24,25]. Below $T_{\alpha\beta}$ and above $T_{\beta\alpha}$, however, the α-form crystal grows faster than the β-form iPP. Both values of $T_{\alpha\beta}$ and $T_{\beta\alpha}$ are dependent on the isotacticity of iPP used [25]; the lower the isotacticity, the lower the transition temperatures of $T_{\alpha\beta}$ and $T_{\beta\alpha}$. For the present system, the crystalline iPS fibers first induce the dense α-form nuclei at its surface during cooling from 200 °C. Despite the rare occurrence of β nucleation in the bulk, the β-form nuclei are likely to be initiated at the growing oriented front of α-form crystals [26]. Subsequent growth of β-form nucleus at the growing TCL front of α crystals may prevail, provided that the temperature is lower than the $T_{\beta\alpha}$. The "fan-like" morphology of β-form crystals as observed in Fig. 6 indicates that few β-nuclei are generated by a cooling rate of 4 °C/min. For this unique α-to-β growth transition, Lotz [27] proposed the requirement of reorientation of one helix of the depositing $(110)_\beta$ plane in contact with the growing $(040)_\alpha$ plane. Based on the above arguments, the formation of β-form iPP should be favored under a fast cooling process because the crystallization temperature of the α-form iPP decreases with increasing cooling rate. On the other hand, a low cooling rate might lead to the full crystallization of α-form iPP prior to reaching the $T_{\beta\alpha}$ to facilitate α/β growth bifurcation. Solid evidence is provided in Fig. 8a and b, showing the POM images of samples cooling at a higher rate of 20 and 60 °C/min, respectively. In contrast to the fan-like β-form in Fig. 6 at a cooling rate of 4 °C/min, "cylindrite-like" [1] β-form crystals are developed around the iPS fibers, indicating that the number of β-form nuclei increases with increasing cooling rate, plausibly due to the development of dense α-form nuclei at the fiber surface. To reveal the effect of internal structure (crystalline or

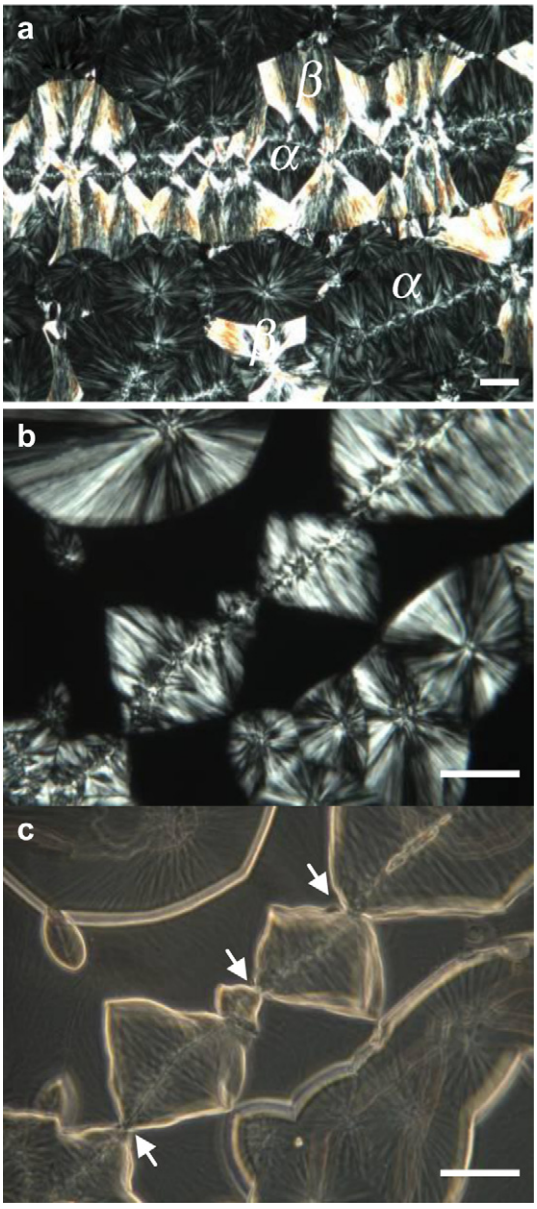

Fig. 6. POM images of (a) iPP filled with electrospun iPS fibers cooled from 200 °C to room temperature at a rate of 4 °C/min and (b) After selective melting of the β-form iPP at 153 °C with a heating rate of 10 °C/min (c) is the phase contrast images of (b) To clearly elucidate the residual α-form thin layer (pointing by arrows) at the fiber surface after the removal of β-form iPP. The scale bar is 200 μm.

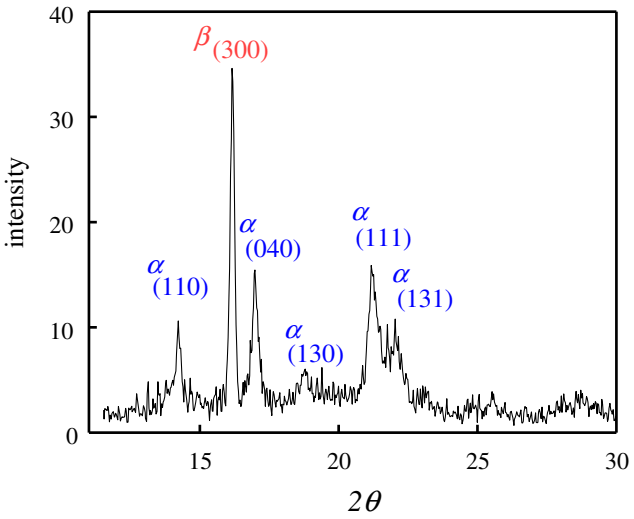

Fig. 7. WAXD intensity profile of iPP thin film filled with electrospun iPS fibers after cooling from 200 °C at 4 °C/min to room temperature. The peak at 2θ of 16.2° is attributed to β (300) plane, whereas those at 14.2, 17.0, 18.8, 21.2, and 22.1° are associated with the α-form of (110), (040), (130), (111) and (131) planes, respectively.

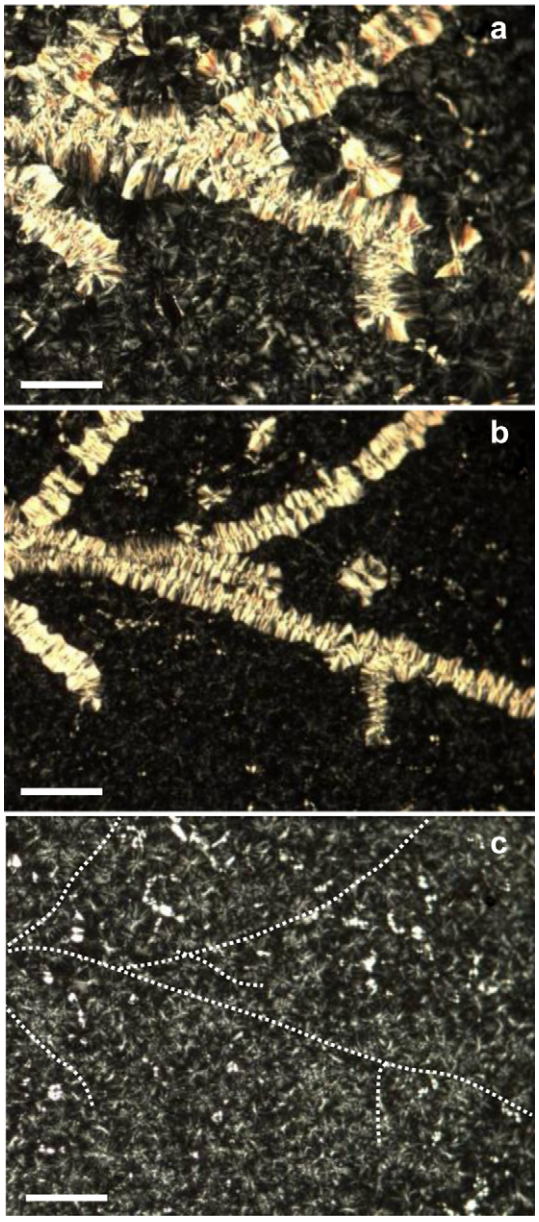

Fig. 8. POM images of iPS fiber-induced crystallization of iPP matrix (a) Holding at 200 °C for 10 min, following by cooling at a rate of 20 °C/min to room temperature, (b) Cooling from 200 °C at a rate of 60 °C/min, (c) Holding at 280 °C for 3 min to melt the iPS fibers, followed by cooling at a rate of 60 °C/min to room temperature. In (c), the dotted lines indicate the fiber locations before fiber melting. The scale bar is 200 μm.

amorphous) on the nucleating ability of iPS fibers, the sample was heated to 280 °C for 3 min, followed by 60 °C/min cooling. Such thermal treatment makes the iPS fibers amorphous, thereby losing their nucleating ability toward iPP, as shown in Fig. 8c. The present findings are significantly different from those reported by Phillips et al. [3], who used powder forms of iPS to induce iPP crystallization. They reported that crystalline iPS powders could induce β-form iPP, whereas amorphous iPS powders yield α-iPP only in the absence of β-iPP. These discrepancies and misleading conclusions might be attributed to the difficulties in visually tracing the nucleation process at the particle surface when the nucleating particles are too small and/or too many. Having a large aspect ratio, electrospun iPS fibers provide a more convenient and reliable observation of nucleation event at the fiber surface, supporting the dual nucleating ability of crystalline iPS fibers. More importantly, amorphous iPS fibers behave in a manner similar to the aPS fibers [5], exhibiting the disability to induce preferential iPP nucleation at its surface. In consideration of the large surface area, iPS nanofibers are more effective and desirable than the spherical iPS particles to act as a nucleating agent for iPP.

Isothermal crystallization was also performed by rapid cooling from 200 °C to various crystallization temperatures (T_c). The maximum temperature (T_{max}) required for TCL to occur is 138 °C, above which no preferential nucleation of iPP takes place at the iPS fiber surface in comparison with the bulk. For the α/β bifurcation of iPP to proceed, the T_c should be lower than 135 °C. Only α-iPP TCL crystals are developed in the T_c range of 136–138 °C. The β-form content of iPP increases with further decrease in T_c. The parameter T_{max} provides a measure of the nucleating ability of a given fiber [5]; the higher the T_{max}, the better the nucleating ability of fibers. Our previous study on the nucleating ability of electrospun sPS fibers showed that the T_{max} for the sPS fibers is 124 °C, and only α-form iPP is induced regardless of the crystallization conditions [5]. Thus, crystalline iPS fibers possess better nucleating ability for iPP than electrospun sPS fibers despite the similar hexagonal crystal modifications with unit cells of $a = b = 2.19$ nm, $c = 0.67$ nm for iPS [28], and $a = b = 2.626$ nm, $c = 0.51$ nm for sPS [29].

3.4. Plausible nucleating mechanism for the iPS fibers

Epitaxial crystallization is widely used to account for the TCL development, provided that a periodicity exists on the fiber surface and the dimension matches the particular spacing of the crystallizing plane of iPP [2]. In general, epitaxy is defined in terms of geometric lattice matching, and 13% mismatching is considered the upper limit for the occurrence of epitaxial growth [30]. Epitaxy of α-form iPP is favored when the fiber surface has a periodicity of ~0.56 and ~0.50 nm; the former may interact with the (110) crystal plane, and the latter accommodates the (040) crystal plane [2]. As shown in Fig. 3a, two broad d-spacings of 0.981 and 0.471 nm exist in the as-spun amorphous iPS fibers. The spacing of 0.471 nm is relevant to the average distance between two phenol rings along the chain direction. This spacing is inactive for iPP crystallization because of the absence of long-range order to host the nuclei of iPP. During annealing, re-organization of the phenol rings takes place to bring about the dense crystallographic plane of (211) reflection at $2\theta = 18.0°$, corresponding to a periodicity of 0.492 nm. This regular dimension at the crystalline iPS fibers matches with the (040) plane of α-form iPP, which might serve as a means to nucleate the α crystal. The overgrowth of (040) plane is confirmed by the WAXD profiles shown in Fig. 7. The subsequent growth of (040) plane is likely to bring up the β-nucleus at its growth front [27] when dense α-form nuclei are placed at the fiber surface at temperatures below $T_{\beta\alpha}$. As regards the as-spun sPS fibers, they are also in amorphous state, exhibiting two amorphous halos with d-spacings of 0.981 and 0.471 nm. On heating to 200 °C, the development of dense (211) crystal plane at $2\theta = 20.1°$ is evidently observed to provide a periodicity of 0.440 nm [20]. The dimensional mismatching is about 12% with the (040) plane of α-form iPP, indicating that epitaxial growth of iPP is more difficult to take place than iPS fibers. We conclude that there is a significant difference in nucleating ability toward iPP between electrospun iPS and sPS fibers despite the similar crystal lattices. It should be reminded that chain conformation in the iPS crystal is 3_1 helix, whereas the sPS chains take all-trans (planar zig-zag) confirmation in the crystalline state. To further explore the deposition of the 3_1 helix chains of iPP, the molecular modeling will be attempted to reveal the conformation of PS chains associated with the (211) plane.

4. Conclusions

Uniform iPS fibers were obtained by electrospinning its solutions with *o*-DCB solvent at 73 °C. The cooled solutions remained homogeneous even at room temperature for hours due to the slow process of gel formation and/or crystallization, which led to the feasibility of ambient electrospinning. However, fibers electrospun from the elevated temperature had lower diameter than those obtained from room temperature because of reduced viscosity. Aligned iPS fibers with diameter of 325 ± 74 nm were also prepared using a rotating disc. The as-spun fibers were in the amorphous state in the absence of a long period. During stepwise annealing, a long period of 13.2 nm was initially detected by SAXS at 140 °C, which increased to 14.6 nm at 200 °C. WAXD results showed that iPS crystals initially appeared at 110 °C, and fiber crystallinity increased with increasing annealing temperatures. Based on the Herman function, the orientation factor of crystal *c*-axis decreased with increasing temperature, being 0.37 at 120 °C and 0.32 at 200 °C. When the iPS nanofibers were embedded in the iPP matrix, surface-induced crystallization took place to develop the mixed α/β crystals. POM observations revealed that dense α-form iPP nuclei cover the fiber surface first, and the β-form nuclei are initiated at some selected locations of the α crystal growing front. The β-growth later becomes dominant due to its high growth rate. In other words, the α to β crystal transformation takes place during TCL growth, which indicates the dual nucleating ability of iPS fibers. The content of β-form iPP depends upon the cooling rate and isothermal crystallization temperature. Isothermal results showed that the T_{max} for the electrospun iPS fibers is about 138 °C, which is higher than that for the electrospun sPS fibers at ~124 °C.

Acknowledgment

This work was financially supported by National Science Council of Taiwan (NSC 98-2221-E-006-005-MY3), and National Synchrotron Radiation Research Center (NSRRC, 2009-2-047-5). The assistance of 2-D SAXS, and 2-D WAXD experiments from Drs. U-Ser Jeng and Jey-Jau Lee in NSRRC is highly appreciated.

Appendix A. Supplementary data

Supplementary data related to this article can be found at http://dx.doi.org/10.1016/j.polymer.2012.09.036.

References

[1] Varga JJ. Macromol Sci Part B- Phys 2002;41:1121.
[2] Mathieu C, Thierry A, Wittmann JC, Lotz B. J Polym Sci Polym Phys 2002;40:2504.
[3] Phillips A, Zhu PW, Edward G. Polymer 2010;51:1599.
[4] Su Z, Dong M, Guo Z, Yu J. Macromolecules 2007;40:4217.
[5] Wang C, Liu FH, Huang WH. Polymer 2011;52:1326.
[6] Pai CL, Boyce MC, Rutledge G. Polymer 2011;52:2295.
[7] Reneker DH, Fong H, editors. Polymeric nanofibers; ACS symposium series 918. Washington, DC: American Chemical Society; 2006.
[8] Ramakrishna S, Kazutoshi F, Teo WE, Lim TC, Ma Z. An introduction to nanofibers. Singapore: World Scientific Co., Pte. Ltd; 2005.
[9] Greiner A, Wendorff JH. Angew Chem Int Ed 2007;46:5670.
[10] Tosaka M, Yamaguchi K, Tsuji M. Polymer 2010;51:547.
[11] Wang C, Hsieh TC, Cheng YW. Macromolecules 2010;43:9022.
[12] Jeng US, Su CH, Su CJ, Liao KF, Chuang WT, Lai YH, et al. J Appl Cryst 2010;43:110.
[13] Alexander LE. X-ray diffraction methods in polymer science. New York: John Wiley & Sons; 1969. 241.
[14] Baltá-Calleja FJ, Vonk CG. X-ray scattering of synthetic polymers. New York: Elsevier; 1989. 247.
[15] Al-Hussein M, Strobl G. Macromolecules 2002;35:1672.
[16] Xu H, Cebe P. Polymer 2005;46:8734.
[17] Turner-Jones A, Aizlewood J, Beckett D. Macromol Chem Phys 1964;75:134.
[18] McKee MG, Wilkes GL, Colby RH, Long TE. Macromolecules 2004;37:1760.
[19] Huang CL, Chen YC, Hsiao TJ, Tsai JC, Wang C. Macromolecules 2011;44:6155.
[20] Cheng YW, Lu HA, Wang YC, Thierry A, Lotz B, Wang C. Macromolecules 2010;43:2371.
[21] Xu H, Ince BS, Cebe P. J Polym Sci Polym Phys Ed 2003;41:3026.
[22] Duan Y, Zhang J, Shen D, Yan S. Macromolecules 2003;36:4874.
[23] Statton WO. J Polym Sci 1956;22:385.
[24] Varga J, Menyhárd A. Macromolecules 2007;40:2422.
[25] Nakamura K, Shimizu S, Umenmoto S, Thierry A, Lotz B, Okui N. Polym J 2008;40:915.
[26] Lovinger AJ, Chua JO, Gryte CC. J Polym Sci Polym Phys Ed 1977;15:641.
[27] Lotz B. Polymer 1998;39:4561.
[28] Natta G, Corradini P, Bassi IW. Nuovo Cimento 1960;15:68.
[29] Gowd EB, Tashiro K, Ramesh C. Prog Polym Sci 2009;34:280.
[30] Lotz B, Thierry A. Polymer crystal: epitaxial growth. In: Buschow KHJ, editor. Encyclopedia of materials: science and Technology, vol. 8. Amsterdam: Elsevier; 2001. p. 7267–72.